ELSEVIER

Surface Science 488 (2001) 90–98

SURFACE SCIENCE

www.elsevier.com/locate/susc

Spin-polarized electron emission induced by impact of protons and electrons on Cr/Fe(1 0 0)

R. Pfandzelter *, M. Ostwald, H. Winter

Institut für Physik, Humboldt-Universität zu Berlin, Invalidenstrasse 110, 10115 Berlin, Germany

Received 14 July 2000; accepted for publication 4 April 2001

Abstract

We report on spin- and energy-resolved secondary electron emission, induced by impact of fast protons and electrons on ultrathin Cr films epitaxially grown on Fe(1 0 0). Based on a simple model, we extract spin- and energy-dependent probing depths from experimental polarization spectra. For grazing impact of protons the probing depth strongly depends on the energy of secondary electrons.

Keywords: Secondary electron emission measurements; Electron emission; Metal–metal magnetic thin film structures; Magnetic surfaces; Single crystal epitaxy; Ion–solid interactions; Iron; Chromium

1. Introduction

When solid surfaces are irradiated with energetic particles like electrons or ions, electrons of predominantly low energy are emitted. These so-called secondary electrons originate from a small region beneath the surface. Analysis of intensity and energy of secondary electrons thus allows one to study properties of surfaces. For excitation with primary electrons of a few keV energy, it has evolved into a standard technique in surface science (secondary electron emission spectroscopy) [1].

In recent years the technique has been extended to the study of magnetic surfaces by performing a spin analysis of emitted electrons [2,3]. This not only yields information on magnetic and electronic properties of surfaces, but also improves our understanding of the electron emission processes. In a number of spin-polarized experiments on ultrathin films, it could be shown that the probing depth amounts to a few atomic layers only and depends on the material [2,4–6], in contrast to previous assumptions [7].

Use of ions in spin-polarized electron emission could bear advantages over conventional excitation by electrons (e.g. magnetic sputter depth profiling [8]), but is still in its infancy, presumably due to the higher experimental complexity. A close relationship with electron-induced electron emission is expected for light ions with high energies (typically a few tens of keV). Here sputter effects are small or absent and the excitation energy stems from the kinetic energy of the ion as in excitation by electrons. Main difference is the scattering process itself. Ions essentially suffer small-angle

* Corresponding author. Tel.: +49-30-2093-7693; fax: +49-30-2093-7899.

E-mail address: pfandz@physik.hu-berlin.de (R. Pfandzelter).

0039-6028/01/$ - see front matter
PII: S0039-6028(01)01109-8

scattering, which is easily calculated using classical mechanics computer simulations. This offers an exciting possibility: ions which are grazingly incident upon a flat surface do not penetrate into the surface, but are specularly reflected ("surface channeling" [9]). Thus electrons should be excited predominantly at the topmost surface layer and the small probing depth in electron emission spectroscopies is reduced further [10,11].

Here we report on spin-polarized electron emission from ultrathin Cr films epitaxially grown on magnetized Fe(1 0 0) surfaces. Electrons are induced either by grazing impact of 25 keV protons or 4 keV electrons at oblique incidence. Both energy and spin of electrons emitted in a direction close to normal are measured as function of the Cr coverage. The purpose of these studies is to obtain information on the magnetic properties of Cr overlayers and to compare features of proton and electron induced electron emission. In particular, we aim to deduce values for the probing depths and their dependence on primary particle as well as energy and spin of emitted electron.

2. Experiment

The experiments are performed in an ultrahigh-vacuum chamber (base pressure 3×10^{-11} mbar), attached via differential pumping stages to the beam line of a small electrostatic ion accelerator. The (1 0 0) face of an Fe single crystal disk (diameter 9 mm) is prepared by many cycles of grazing sputtering (incidence angle to the surface plane about 3°) with 25 keV Ar^+ ions and subsequent annealing (960 K) until the surface is clean and well-ordered, as checked by low-energy electron diffraction (LEED) and Auger electron spectroscopy. From characteristic features in the angular distribution of grazingly scattered ions affected by surface steps [12], we deduce a mean terrace width of more than 1000 Å.

The Fe crystal is mounted to close the gap of a soft-magnetic FeCo yoke with a coil. The crystal is magnetized by current pulses through the coil along an easy axis of magnetization [0 0 1] or [0 0 $\bar{1}$] in the (1 0 0) surface plane and perpendicular to the scattering plane defined by the proton beam and the surface normal. This reproducibly yields a full remanent magnetization as checked by the longitudinal magneto-optic Kerr effect. Scanning an electron beam over the target surface and measuring the spin polarization of secondary electrons indicates a uniform magnetization (single domain structure) near the center and a roughly 20% reduction towards the edges. External magnetic fields are compensated by three pairs of Helmholtz coils to a few μT.

Cr is deposited from a high-purity tapered piece by electron beam heating in a commercially available evaporator (EFM3, Omicron). Adjustment and continuous control of the flux are allowed by a shutter and an integrated flux monitor. Growth is monitored in situ and in real time by measuring the specular intensity of grazingly scattered ions [13]. This technique enables one to calibrate the flux monitor of the evaporator and quantitatively determine the morphology of the film surface. For the present studies we choose a growth temperature of about 610 K, where growth is found to proceed in an almost perfect layer-by-layer mode, in agreement with our previous studies [14]. Typical growth rates are some 10^{-4} ML s^{-1}. During deposition the background pressure did not rise above 1×10^{-10} mbar.

Electrons are emitted either by 25 keV protons or by 4 keV electrons. The well-collimated proton beam (angular divergence $\pm 0.02°$) is incident upon the target at a grazing angle of 1.2° to the surface plane along a high-index surface lattice direction ("random azimuthal orientation"). The incidence angle of the electron beam is 33°. Emitted electrons are collected within a cone of about 12° full opening angle around a direction of 10° off normal and enter a cylindrical sector field energy analyzer via a transfer lens (CSA300, Focus). After energy separation and 90° deflection, electrons are imaged by another lens into a LEED spin-polarization detector [15] (SPLEED, Focus). Pass energy (80 eV), energy resolution (3.0 eV FWHM), and LEED scattering energy (104.5 eV) are kept constant during energy scans. Primary currents (typically 100 nA) and electron count rates (some 10^4 s^{-1}) are comparable for proton and electron excitation. Source area and luminosity are given

by geometry and are therefore different (typically 1×9 and 2×2 mm^2, respectively).

For the measurements the target is kept in a remanent state of magnetization. Each polarization spectrum is obtained from two identical measurements with reversed magnetization to eliminate instrumental asymmetries (typically 20%) and checked by measurements on a paramagnetic Ta foil attached directly near the Fe target. The spin polarization P is calculated by a cross-multiplication of the counts N_1 and N_2 in counter 1 and 2, respectively,

$$P = \frac{1}{S} \frac{\sqrt{N_1^{\uparrow} \cdot N_2^{\downarrow}} - \sqrt{N_2^{\uparrow} \cdot N_1^{\downarrow}}}{\sqrt{N_1^{\uparrow} \cdot N_2^{\downarrow}} + \sqrt{N_2^{\uparrow} \cdot N_1^{\downarrow}}}, \quad (1)$$

where $\uparrow$ and $\downarrow$ refer to the direction of magnetization and $S \approx 0.2$ is the effective Sherman function [16].

In order to discriminate secondary electrons generated at surfaces in the chamber other than the target surface, we biased the target by -10 V with respect to ground [17]. Moreover, this causes an increase of the effective solid angle at small electron energies, which at least partly compensates for the energy dependence of the transmission due to residual magnetic stray fields. The former effect is estimated from numerical calculations of electron trajectories to 30% at 5 eV (20% at 10 eV) and qualitatively confirmed by intensity measurements using different bias voltages. It is not corrected, since we are interested in normalized intensity differences.

3. Experimental results

In Fig. 1 we show intensity distribution (curves) and spin polarization (open and solid circles) of electrons emitted by impact of protons (a) and electrons (b) upon the clean and Cr-covered Fe(1 0 0) surface, respectively. The spectra were recorded at 610 K during film growth. The intensity distributions in Fig. 1 (curves) are normalized to the intensity at 20 eV. They exhibit the well-known behavior: a pronounced peak with a maximum at 1–2 eV and a gradual decrease towards

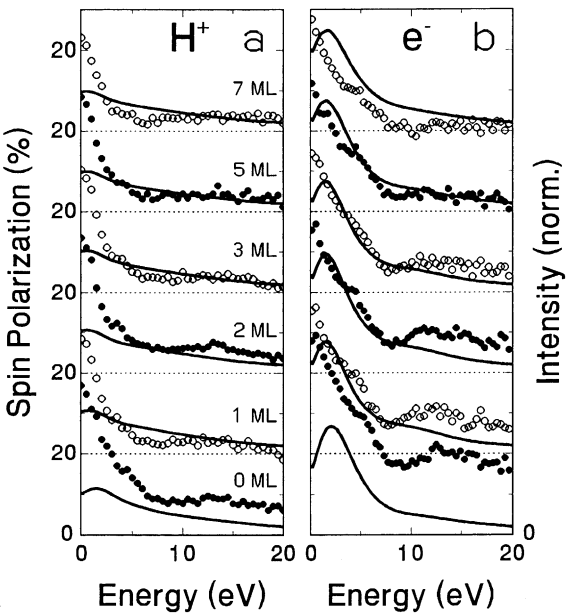

Fig. 1. Intensity distribution (curves, right-hand ordinate) and spin polarization (symbols, left-hand ordinate) of electrons excited by (a) 25 keV protons and (b) 4 keV electrons. The spectra refer to the clean Fe(1 0 0) surface (bottom) and Cr coverages (±0.2 ML in each case) as indicated. The intensity distributions are normalized to the intensity at 20 eV. The origins are displaced vertically by constant amounts (- - -).

higher electron energies. The peak is ascribed to cascade multiplication owing to kinetic electron–electron collisions. The cascade peak is less pronounced in the normalized distribution for proton impact. We attribute this to an enhanced contribution from direct collisions between projectile and electrons. In fact, previous studies on angle-resolved proton-induced electron emission from Al have shown that direct kinetic emission leads to a broad peak at about 10 eV (for our direction of emission) [20].

The effect of the Cr coverage on the intensity distributions is weak, aside from a shift of the maximum to smaller energies. During growth of the first ML, the maximum gradually shifts from 2.0 to 1.5 eV (from 1.5 to 0.9 eV) for electron (proton) excitation (Fig. 2, solid circles). As proposed by Chung and Everhart, this indicates a decrease in work function [21]. From the photothreshold for electron emission upon irradiation with UV photons, we obtain a mean work function

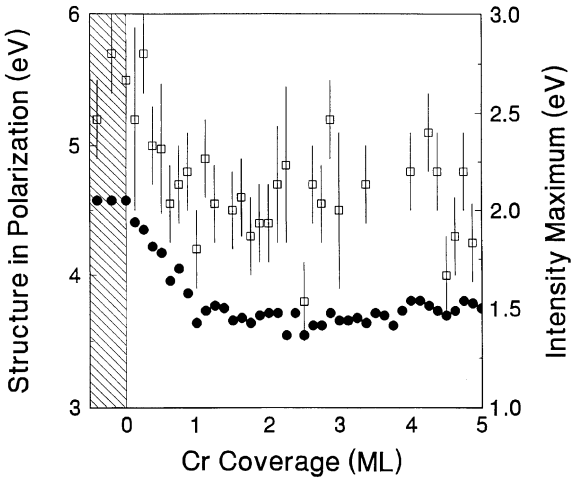

Fig. 2. Energetic positions of intensity maximum (•) and fine structure in the spin-polarization curve (□) for impact of 4 keV electrons. The fine-structure positions are derived from maxima of the second derivative d^2P/dE^2 of smoothed polarization curves.

of 4.4 eV for the clean Fe(1 0 0) surface and 4.1 eV for 1 ML Cr overlayer.

The observed spin polarization (Fig. 1, circles) is in agreement with previous studies on electron-induced electron emission [22,23]: It is largest for small energies and falls rapidly within the range of cascade electron energies (Fig. 1b). This is also observed for proton excitation (Fig. 1a). This similarity between proton and electron excitation is remarkable, as it shows that cascade effects are important even for grazing angles of incidence.

For the clean Fe surface, the polarization is smaller for proton impact than for electron impact. So far, it is not clear whether this difference has to be ascribed to different excitation mechanisms. Conceivable effects are the large source area (reduced magnetization near the sample edge) and the smaller probing depth for proton excitation. In fact, we observe a pronounced thermal decrease of the polarization (about 0.7) upon heating from room temperature to 610 K. This is not observed for electron excitation.

Superimposed on the smooth cascade part of the polarization spectra are fine structures at about 5 and 13 eV, the latter apparently related to a slight hump in the (electron-induced) intensity distribution. These features have been observed previously on Fe(1 1 0) [17] and attributed to the spin-dependent band structure [24] and the crystallinity of the sample [17], respectively. Upon growth of Cr, the 5 eV structure shifts by about 1 eV to smaller energies (Fig. 2, open squares). The 13 eV structure weakens beyond a few ML. This may be related to a deterioration in crystallographic order (e.g. kinetic roughening of the film).

The dependence of the values of the polarization on the Cr coverage is significantly different for proton and electron excitation. Whereas a gradual decrease is observed for primary electrons, impact of protons results in a nonmonotonic dependence. For example, the polarization increases upon deposition of the second layer on top of 1 ML Cr/Fe. The effect becomes more evident, when the measured spin polarizations are averaged over a range of electron energies and plotted against the coverage. For proton excitation (Fig. 3, symbols) the behavior strongly depends on the chosen energy interval. For electron energies above a few eV, the spin polarization follows a series of roughly linear variations with break points at integer ML coverages (Fig. 3, squares and circles). However, at small energies (Fig. 3, diamonds), the behavior resembles the polarization observed for electron excitation (Fig. 4, symbols). This is surprising, as it indicates that the probing depth for grazing impact of protons strongly depends on the electron energy sampled. Whereas beyond the range of cascade energies the oscillatory behavior suggests a sensitivity to the topmost film layer, the probing depth seems to be similar to electron excitation at small energies.

We note that the oscillatory behavior of the spin polarization observed for proton excitation closely resembles data obtained by Walker et al. [25] using spin-polarized electron energy-loss spectroscopy. This is another technique with a very small probing depth [3]. The exchange asymmetry oscillates with the film thickness. However, it does not change the sign, which is in accordance with a net ferromagnetic moment at the topmost film layer. A ± oscillatory behavior indicating layer-by-layer antiferromagnetic ordering [26–29] reminiscent of antiferromagnetic bulk Cr seems to evolve for thicker films (Cr coverages beyond 8 ML).

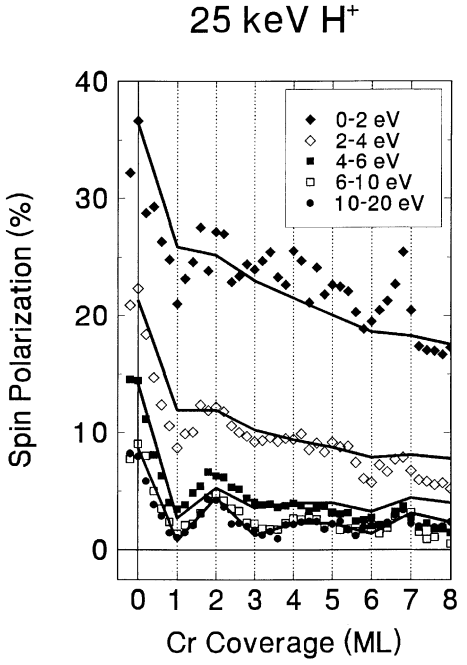

Fig. 3. Measured spin polarization (symbols) of electrons excited by grazing impact of 25 keV protons on Cr/Fe(1 0 0) versus Cr overlayer thickness. Different symbols refer to values averaged over spectral ranges as indicated. The solid lines are results of calculations (Eqs. (2), (4) and (5)) for layer-dependent magnetic moments from Fig. 5 and the following parameters (from bottom to top): $\lambda_s = \lambda_a = 0.5$ ML, $A_s = A_a = 0$, $f = 2.2$; $\lambda_s = 0.4 \times 4.2$ ML, $\lambda_a = 0.4 \times 2.9$ ML, $A_s = 0.25 \times 0.28$, $A_a = 0.25 \times 0.16$, $f = 1.9$; $\lambda_s = 0.8 \times 4.2$ ML, $\lambda_a = 0.8 \times 2.9$ ML, $A_s = 0.55 \times 0.28$, $A_a = 0.55 \times 0.16$, $f = 1.7$; $\lambda_s = 4.2$ ML, $\lambda_a = 2.9$ ML, $A_s = 0.28$, $A_a = 0.16$, $f = 1.3$.

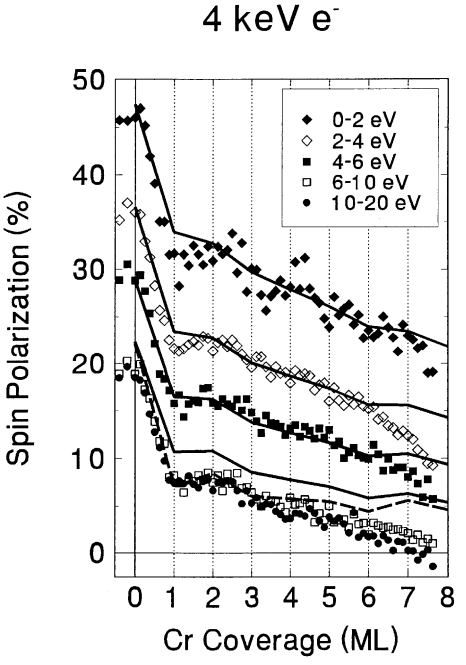

Fig. 4. Same as Fig. 3 for impact of 4 keV electrons. The calculations are performed with mean free paths $\lambda_s = 4.2$ ML, $\lambda_a = 2.9$ ML, $f = 1$ and asymmetries A_s and A_a from Fig. 3. For the dashed line we assumed smaller mean free paths $\lambda_s = 3$ ML, $\lambda_a = 2$ ML.

4. Evaluation of data

For a quantitative understanding of the observed spin polarization and its dependence on electron energy and Cr coverage (Figs. 3 and 4), we perform simple model calculations. The measured spin polarization P is given by

$$P = \frac{I^{\uparrow} - I^{\downarrow}}{I^{\uparrow} + I^{\downarrow}} = \frac{I_s^{\uparrow} + I_a^{\uparrow} - I_s^{\downarrow} - I_a^{\downarrow}}{I_s^{\uparrow} + I_a^{\uparrow} + I_s^{\downarrow} + I_a^{\downarrow}}, \tag{2}$$

where $I^{\uparrow(\downarrow)}$ is the intensity of electrons in the beam with magnetic moment parallel (antiparallel) to the target magnetization and $I_s^{\uparrow(\downarrow)}$ and $I_a^{\uparrow(\downarrow)}$ are the contributions from substrate and film, respectively. For a uniform indepth generation of excited electrons the contribution $I_i^{\uparrow(\downarrow)}$ from layer i to $I^{\uparrow(\downarrow)}$ can be written as

$$I_i^{\uparrow(\downarrow)} = c\, n_i^{\uparrow(\downarrow)}\, n_A \exp(-\sigma^{\uparrow(\downarrow)} z_i) = \frac{1}{2}\, c\, (n_i + (-) n_{B,i})\, n_A \exp(-\sigma^{\uparrow(\downarrow)} z_i), \tag{3}$$

with $n_i^{\uparrow(\downarrow)}$ the number of majority (minority) spin electrons in the conduction band, n_i the total number of conduction (d and sp) electrons and $n_{B,i}$ the Bohr magneton number. $+(-)$ stands for $\uparrow(\downarrow)$. n_A is the density of atoms and c a proportionality constant. z_i is the depth below the surface and $\sigma^{\uparrow(\downarrow)}$ the (spin-dependent) total scattering cross-section.

The contribution from film $I_a^{\uparrow(\downarrow)}$ is obtained by summing over all film layers

$$I_a^{\uparrow(\downarrow)} = \sum_i \frac{1}{2}\, c\, (n_{a,i} + (-) n_{Ba,i})\, n_A \exp(-\sigma_a^{\uparrow(\downarrow)} z_i), \tag{4}$$

where $n_{Ba,i}$ and, in the case of interfacial alloying, $n_{a,i}$ are layer dependent. Assuming a constant

magnetization in the substrate (n_{Bs} independent of the layer), the total substrate contribution $I_s^{\uparrow(\downarrow)}$ is given by

$$I_s^{\uparrow(\downarrow)} = \frac{1}{2}\, c' \,\frac{n_s + (-)n_{Bs}}{\sigma_s^{\uparrow(\downarrow)}}\, n_A \exp(-\sigma_a^{\uparrow(\downarrow)} d) \tag{5}$$

with film thickness d. Note that n_A is the same for film and substrate for pseudomorphic growth. With $c = c'$, insertion of Eqs. (4) and (5) in Eq. (2) allows one to calculate the spin polarization P from the layer-dependent Bohr magneton numbers $n_{Ba,i}$, if the scattering cross-sections are known.

A compilation of experimental data by Schönhense and Siegmann [5,6] suggests that the scattering cross-sections at small electron energies ($E < 5$ eV) cannot be described by a universal behavior [7], but are material dependent. For transition metals σ increases proportional to the number of holes ($10-n_d$) in the d-bands (n_d is the number of d-electrons),

$$\sigma = \sigma_0 + \sigma_d \tfrac{1}{2}(10 - n_d), \tag{6}$$

where σ_0 accounts for inelastic scattering other than into the d-band holes. Extension to magnetic materials is straightforward

$$\sigma^{\uparrow(\downarrow)} = \sigma_0 + \sigma_d \left(5 - n_d^{\uparrow(\downarrow)}\right) \tag{7}$$

with spin dependent cross-sections $\sigma^{\uparrow(\downarrow)} = \sigma(1 - (+)A)$ and asymmetry A. This asymmetry in scattering cross-sections gives rise to a transport polarization, which is acquired by electrons travelling through a ferromagnetic material.

Following the common practice we discuss our results in terms of the inelastic mean free path $\lambda = 1/\sigma$. Often this term is merely used as a phenomenological probing depth describing the exponential attenuation of intensities as in Eq. (3) [30]. We adopt this terminology, as it includes possible elastic scattering and cascade effects. In particular a generalization to grazing proton impact is possible, where the polarization should be determined by the excitation depths of electrons rather than their transport to the surface (''spin-filter effect'').

For small electron energies $E < 5$ eV and a uniform indepth generation of excited electrons as for electron impact, we adopt from Refs. [5,6] $\lambda_s = 6.0$ Å $= 4.2$ ML for Fe and $\lambda_a = 4.2$ Å $=$ 2.9 ML for Cr. Adjusting $\sigma_0/\sigma_d = 2.5$ to experimental results yields for Fe $A_s = 0.28$, i.e. $\lambda_s^{\uparrow} = 5.8$ ML and $\lambda_s^{\downarrow} = 3.3$ ML.

When grazingly incident protons are used as primary particles instead of electrons, the depth distribution of excited electrons should be reduced significantly. In the ideal case of perfect specular reflection we expect $\lambda^{\uparrow} = \lambda^{\downarrow} = \lambda \to 0$ and $A \approx 0$, independent of the chemical composition of the surface. Yet there is a finite probability for the protons to penetrate the surface via ledges of islands, substrate step edges or thermally displaced atoms. From trajectory simulations on the scattering of protons from imperfect surfaces [12], we estimate $\lambda = (0.5 \pm 0.3)$ML.

In Eqs. (2) and (3) it is tacitly assumed that the observed spin polarization directly reflects the spin part of the magnetization $M_s = n_B\, \mu_B\, n_A$. Although this seems to hold for excitation with keV electrons (for Fe $P \approx n_B/n = 2.13/8 = 26.6\%$ beyond the secondary cascade peak [31]), the polarization of emitted electrons surely depends on how the energy is supplied to the conduction electrons. Studies on the primary energy dependence show that the polarization strongly decreases below 1 keV primary electron energy [18,19]. When ions are used as primary particles, Kirschner et al. observed that the polarization is smaller compared to excitation with isoenergetic electrons [8]. To consider that the relative probability of electron emission from various electron states depends on the way of excitation, we therefore introduce a prefactor f in Eq. (2) ($f \approx 1$ for excitation with keV electrons) [2].

5. Discussion

We first deduce the layer-dependent magnetic moments of the Cr films $n_{Ba,i} \cdot \mu_B$ from a fit to the proton-induced data for 10–20 eV (Fig. 3, solid circles), using Eqs. (2), (4) and (5). This is straightforward, since the probing depth is small (subsurface layers hardly contribute to the signal) and should not depend on spin direction or surface layer composition ($\lambda_s^{\uparrow} = \lambda_s^{\downarrow} = \lambda_a^{\uparrow} = \lambda_a^{\downarrow} \approx 0.5$ ML).

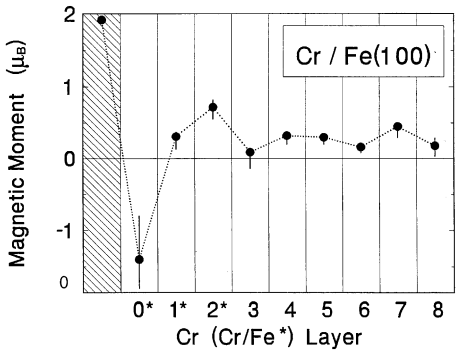

Fig. 5. Magnetic moment per atom at the topmost film layer versus total number of Cr layers on Fe(1 0 0), obtained from a fit to the data from Fig. 3 (10–20 eV) according to Eqs. (2), (4) and (5). Alloyed layers are marked by $*$ (0^* and 1^* refer to the subsurface and surface layer after deposition of 1 ML of Cr, respectively).

To take account of interfacial alloying (50%/50% Cr/Fe for subsurface and surface layer after deposition of 1 ML and 75%/25% Cr/Fe for the surface layer at 2 ML Cr [32,33]), we calculate $n_{a,0}$, $n_{a,1}$, $n_{a,2}$ from elemental values $n_s = 8$ and $n_a = 6$. The magnetic moments obtained are shown in Fig. 5. As expected, they closely follow the measured spin polarization curve. A discussion of this magnetization profile can be found elsewhere [34], where the same profile (within our error bars) has been inferred, although from a larger energy range.

Turning to smaller electron energies, we face the problem of several unknown fitparameters. In fact, the similarity to electron-induced data suggests larger probing depths λ and, consequently, non-vanishing asymmetries A. We therefore turn to the lowest-energy data (0–2 eV) for excitation by electrons (Fig. 4, solid diamonds). Here we can take the values from Section 4 ($\lambda_s = 4.2$ ML, $\lambda_a = 2.9$ ML, $A_s = 0.28$ and $f = 1$). This correctly reproduces the polarization observed for the clean Fe surface.

For the Cr film we adopt the magnetization profile from Fig. 5 and an asymmetry A_a as single fit parameter. Best agreement is obtained for $A_a = 0.16$ (Fig. 3, topmost solid line). A positive transport polarization in the Cr film seems reasonable, considering a predominant positive magnetization (Fig. 5). Of course, a constant A_a does not take account of layer-by-layer oscillations of Cr moments. Consequently, the polarization at 1 ML coverage is overestimated.

In order to reproduce the decreasing polarization at higher electron energies, we have to reduce the asymmetry A_s, whereas the probing depth λ and $f = 1$ can be expected to remain unchanged. For 2–4 eV (Fig. 4, open diamonds), best agreement is obtained with $A_s = 0.55 \times 0.28$ (and $A_a = 0.55 \times 0.16$). For 4–6 eV (Fig. 4, solid squares), we get $A_s = 0.25 \times 0.28$. This trend continues for even higher energies (Fig. 4, open squares, solid circles), where $A_s = 0$.

For energies $E > 6$ eV the calculated curve lies above the measured values by about 2%. Excluding systematic experimental errors, this indicates smaller probing depths. Reasonable agreement is obtained for $\lambda_s \approx 3$ ML and $\lambda_a \approx 2$ ML (Fig. 4, dashed line). A reduction of the (spin-averaged) mean free path towards higher energies is in line with the general trend displayed in the so-called "universal curve", where the probing depth runs through a minimum at an energy of a few tens of eV [7].

Turning back to proton impact, the low-energy data (Fig. 3, solid and open diamonds, solid squares) are easily fitted adopting the energy-dependent asymmetries A_s, A_a from Fig. 4. We obtain $\lambda_s = 0.4 \times 4.2$ ML, $\lambda_a = 0.4 \times 2.9$ ML and $f = 1.9$ for 4–6 eV, 0.8×4.2 ML, 0.8×2.9 ML, $f = 1.7$ for 2–4 eV and 4.2 ML, 2.9 ML, $f = 1.3$ for 0–2 eV. Thus the probing depth for grazing proton impact significantly increases towards very small energies. This shows that proton excitation resembles electron excitation in the range of cascade electron energies. Since the excitation depths are clearly different, we conclude that subsurface layers are involved in the development of the secondary electron cascade. Electrons excited by protons within the topmost layer produce excited electrons in subsurface layers by electron–electron scattering. This accumulation of excited electrons grows considerably with decreasing energy [35].

The iterative procedure in fitting our experimental results is possible, because the effects of mean free path and spin asymmetry on the spin polarization of emitted electrons are different. This

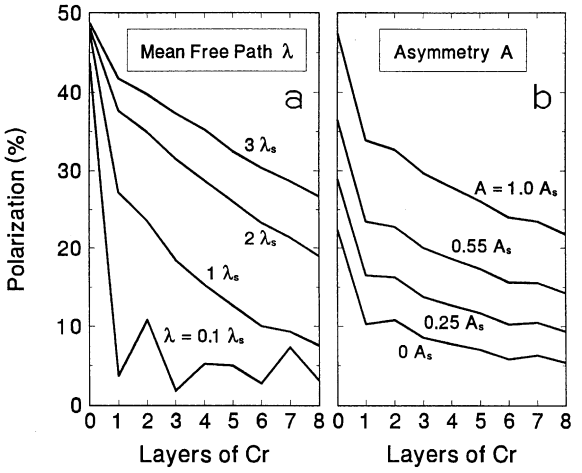

Fig. 6. Calculated spin polarization (Eqs. (2), (4) and (5)) with layer-dependent magnetic moments from Fig. 5. (a) Variation of mean free paths λ_s, λ_a with constant asymmetries ($A_s = 0.28$, $A_a = 0$). (b) Variation of asymmetries A_s, A_a with constant mean free paths ($\lambda_s = 4.2$ ML, $\lambda_a = 2.9$ ML).

is elucidated in Fig. 6, where calculations have been compiled for different values of λ (a) and A (b), respectively. Whereas the asymmetry A critically affects the polarization value, the probing depth λ determines the shape of the polarization curves. In fact, an oscillatory behavior, as observed for proton impact at larger electron energies, evolves only for small values of λ.

6. Summary and conclusions

In this work we report on spin- and energy-resolved electron emission from ultrathin Cr films on Fe(1 0 0) surfaces. The Cr films were grown under conditions where growth is almost perfectly layer-by-layer and the chemical composition across the interface is known. In addition to conventional excitation by electrons, we used grazing impact of fast protons. For proton excitation, the observed spin polarization strongly depends on the energy of emitted electrons. For energies beyond the secondary electron cascade the polarization follows a series of linear variations with break points at integer ML coverages. For cascade electrons, however, the results are similar for proton and electron impact and the polarization gradually decreases with increasing Cr coverage.

Based on a proportionality between observed spin polarization and spin part of the magnetization and an exponential attenuation of excited electron within film and substrate, we are able to fit the experimental data by adjusting (effective) probing depths. Our results show that the probing depth depends both on the spin and the energy of electrons. The spin dependence, expressed in terms of an asymmetry A in probing depth λ, is maximum below 2 eV. The value $A = 0.28$ agrees with published data [5]. Towards higher energies, A decreases to about zero for $E > 10$ eV (Fig. 7, solid diamonds).

The probing depths λ are clearly different for proton and electron excitation. For electron impact $\lambda \approx 4.2$ ML, with a possible slight reduction towards higher secondary electron energies (Fig. 7, open circles). In contrast, the probing depths for proton impact gradually decrease to very small values (about 0.5 ML) for $E > 10$ eV (Fig. 7, solid circles). This finding implies important consequences: the probing depth in conventional electron induced electron emission spectroscopy can be significantly reduced by use of grazing proton impact, in case emitted electrons are measured energy-resolved. For low-energy cascade electrons, the probing depths approach values for electron impact.

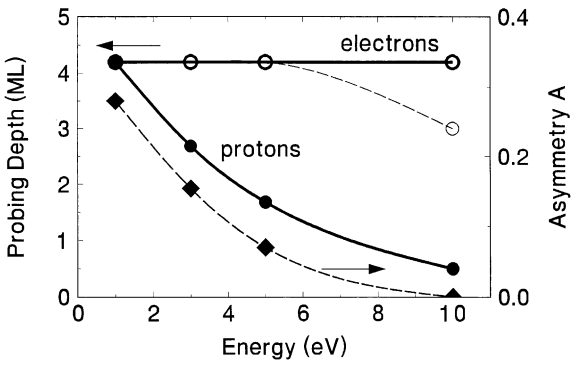

Fig. 7. Probing depths as function of electron energy for proton (●) and electron (○) excitation, respectively (left-hand ordinate). Asymmetry A of spin-dependent scattering cross-sections as function of electron energy (◆, right-hand ordinate).

The extreme sensitivity to the topmost surface layer for proton impact enables one to deduce the layer-dependent magnetization profile of the Cr films in a straightforward manner. This is hardly possible for electron impact due to the spin- and energy-dependent background from subsurface layers. In particular, our results indicate that a quantitative evaluation of electron-induced spin-resolved electron emission experiments is difficult without energy resolution.

Acknowledgements

We thank T. Igel, A. Laws, K. Maass, and R.A. Noack for their assistance in the preparation of experiments. This work was supported by the Deutsche Forschungsgemeinschaft (Sonderforschungsbereich 290).

References

[1] H. Seiler, J. Appl. Phys. 54 (1983) R1.
[2] H.C. Siegmann, J. Phys.: Condens. Matter 4 (1992) 8395, 1992.
[3] H. Hopster, H.C. Siegmann, E. Kay, in: J.A.C. Bland, B. Heinrich (Eds.), Ultrathin Magnetic Structures I, Springer, Berlin, 1994, p. 123.
[4] D.P. Pappas, K.-P. Kämper, B.P. Miller, H. Hopster, D.E. Fowler, C.R. Brundle, A.C. Luntz, Z.-X. Shen, Phys. Rev. Lett. 66 (1991) 504.
[5] G. Schönhense, H.C. Siegmann, Ann. Physik 2 (1993) 465.
[6] H.C. Siegmann, Surf. Sci. 307 (1994) 1076.
[7] M.P. Seah, W.A. Dench, Surf. Interf. Anal. 1 (1979) 2.
[8] J. Kirschner, K. Koike, H.P. Oepen, Phys. Rev. Lett. 59 (1987) 2099.
[9] D.S. Gemmell, Rev. Mod. Phys. 46 (1974) 129.
[10] C. Rau, K. Waters, N. Chen, Phys. Rev. Lett. 64 (1990) 1441.
[11] R. Pfandzelter, J. Landskron, Phys. Rev. Lett. 70 (1993) 1279.
[12] R. Pfandzelter, Phys. Rev. B 57 (1998) 15496.
[13] R. Pfandzelter, T. Igel, H. Winter, Phys. Rev. B 62 (2000) R2299.
[14] R. Pfandzelter, T. Igel, H. Winter, Surf. Sci. 375 (1997) 13.
[15] J. Kirschner, Polarized Electrons an Surfaces, Springer, Berlin, 1985.
[16] J. Kessler, Polarized Electrons, Springer, Berlin, 1985, p. 233.
[17] J. Kirschner, K. Koike, Surf. Sci. 273 (1992) 147.
[18] O. Paul, M. Taborelli, M. Landolt, Surf. Sci. 211/212 (1989) 724.
[19] K. Koike, J. Kirschner, J. Phys. D: Appl. Phys. 25 (1992) 1139.
[20] A. Hegmann, R. Zimny, H.W. Ortjohann, H. Winter, Z.L. Mišković, Europhys. Lett. 26 (1994) 383.
[21] M.S. Chung, T.E. Everhart, J. Appl. Phys. 45 (1974) 707.
[22] J. Unguris, D.T. Pierce, A. Galejs, R.J. Celotta, Phys. Rev. Lett. 49 (1982) 72.
[23] H. Hopster, R. Raue, E. Kisker, G. Güntherodt, M. Campagna, Phys. Rev. Lett. 50 (1983) 70.
[24] E. Tamura, R. Feder, Phys. Rev. Lett. 57 (1986) 759.
[25] T.G. Walker, A.W. Pang, H. Hopster, S.F. Alvarado, Phys. Rev. Lett. 69 (1992) 1121.
[26] J. Unguris, R.J. Celotta, D.T. Pierce, Phys. Rev. Lett. 69 (1992) 1125.
[27] D.T. Pierce, R.J. Celotta, J. Unguris, Phys. Rev. Lett. 73 (1993) 6201.
[28] A. Davies, J.A. Stroscio, D.T. Pierce, R.J. Celotta, Phys. Rev. Lett. 76 (1996) 4175.
[29] A. Davies, J.A. Stroscio, D.T. Pierce, J. Unguris, R.J. Celotta, J. Magn. Magn. Mater. 165 (1997) 82.
[30] C.J. Powell, Surf. Sci. 299/300 (1994) 34.
[31] E. Kisker, W. Gudat, K. Schröder, Solid State Commun. 44 (1982) 591.
[32] D. Venus, B. Heinrich, Phys. Rev. B 53 (1996) R1733.
[33] R. Pfandzelter, T. Igel, H. Winter, Phys. Rev. B 54 (1996) 4496.
[34] R. Pfandzelter, M. Ostwald, H. Winter, Phys. Rev. B 63 (2001) 140406 (R).
[35] M. Rösler, W. Brauer, Particle Induced Electron Emission I, Springer, Berlin, 1991, p. 1.